진동특성치의 변화를 통한 교량의 손상발견

Damage Detection in Highway Bridges Via Changes in Modal Parameters

김 정 태* 류 연 선**
Kim, Jeong-Tae Ryu, Yeon-Sun

ABSTRACT

In highway bridges robust damage detection exercises are mandatory to secure the safety of the structures from hostile environmental conditions such as fatigue, earthquake, wind, and corrosion. This paper presents a damage detection practice in a full-scale highway bridge by utilizing modal response parameters of as-built and damaged states of the structure. First, the test structure is described and modal testing procedures are outlined. Next, a damage detection model which yields information on the location of damage directly from changes in mode shapes is outlined. Finally, the damage detection model is implemented to predict the location of damage in the test structure. From the results, it was found that the damage detection model accurately locates damage in the test structures for which modal parameters of only a single mode are available for pre-damage (as-built) and post-damage stages.

1. INTRODUCTION

Nondestructive damage detection is an important subproblem of rational damage assessment which should be formed on the basis of any decision to repair, rehabilitate, or replace a bridge. During the past decade, a significant amount of research has been conducted in the area of damage detection via changes in the modal responses of structures. For example, research studies have related changes in eigenfrequencies to changes in beam properties[1] and located defects in beam elements from changes in eigenfrequencies[2]. Research studies have also attempted to monitor the integrity of offshore platforms[3], to detect changes in structural integrity of bridges[4], and to estimate damage in large space structures by using changes in modal parameters[5]. Despite the combined research efforts, outstanding needs remain to locate and estimate the severity of damage in the environment of the reality of being capable of measuring only a few vibrational modes and limited structural properties (e.g., geometry and boundary conditions) particularly in large structures.

In this paper, we present a damage detection practice in a full-scale highway bridge by utilizing changes in modal response parameters of as-built and damaged states. We first describe the test structure and modal testing results. Next, we outline a damage detection model which yields information on the damage localization directly from changes in mode shapes between pre-damage (as-built) and post-damage stages. Finally, we implement the damage detection model to predict the location of damage in the test structure. In this study, we limit the use of modal information to a single mode which is the first flexural mode of the test bridge.

* 부산수산대학교 해양공학과 전임강사
** 부산수산대학교 해양공학과 교수

2. MODAL TESTING IN TEST STRUCTURE

2.1 Test Structure

The test structure selected is a plate-girder bridge on the US Interstate Highway I-40 over the Rio Grande river, Bernalillo County, New Mexico, USA (See Fig. 1). The structure was built circa 1963 under the jurisdiction of the New Mexico Standards and Specifications (1954 Edition). Fig. 2(a) shows an elevation view of the tested unit of the bridge span 423 feet: two spans of approximately 130 feet each and a span of approximately 163 feet. Fig. 2(b) shows boundary conditions between spans of the bridge. As schematized in Fig. 2(c), the superstructure of the bridge consists of the deck, the deck supporting system and the bents. The substructure of the bridge consists of a footing which supports the bents and acts simultaneously as a pile cap for a bank of piles. The substructure is in a soil environment which consists of typically a 3 feet layer of clay at the river bed, a 5 feet layer of sand, a 10 feet layer of gravel in sand, a 5 feet layer of compacted clay, and at least a 20 feet layer of compacted sand.

2.2 Dynamic Modal Testing

From August 31, through September 11, 1993 a series of forced vibration tests were conducted on the I-40 bridge by a joint research team (New Mexico State Univ./Ros Alamos National Lab./Texas A&M Univ.). When these tests were performed, temperatures ranged from morning lows 56 degrees F to afternoon highs 80 degrees F. Wind, although not measured, was not considered significant during these tests. Twenty-six accelerometer locations which include 13 along the south girder (i.e., S1-S13) and 13 along the north girder (i.e., N1-N13) are indicated in Fig. 3. At each axial location, a one-inch square aluminum mounting block, on which an accelerometer was mounted, was dental cemented to the inside web of the plate girder at the mid-height. Within a span the three blocks were equally spaced in the axial direction. Blocks at two locations N10 and S10 (shown in Fig. 3) were mounted directly to the splice plates (shown in Fig. 2(a)) on the girder.

A shaker (consisted of a 21,700 lb. reaction mass supported by three air springs resting on top of 55 gallon drums filled with sand) was located at the location S3. A 2200 lb hydraulic actuator bolted under the center of the mass and anchored to the top of the bridge deck provided the input force to the bridge. A random signal generator was used to produce a uniform random signal that was band-passed between 2 and 12 Hz before inputting the signal to the amplifier. A sinusoidal signal generator provided the stepped sign input. The amplifier gain was controlled manually to provide 500 lb. peak sinusoidal force input or an approximately 2000 lb. peak random force input. An accelerometer mounted on the reaction mass was used to measure the force input to the bridge. After all, a data acquisition system was set up to measure acceleration-time histories and calculate FRFs and Power Spectra.

Four levels of damage were inflicted to the midspan of the north plate-girder close to N7 as shown in Fig. 3. The damage that was intended to simulate fatigue cracking was introduced by making various torch cuts. Pre-damage and post-damage accelerometer readings were taken before and after damaging episodes. The modal analysis results for the first bending mode of the bridge are summarized in Table 1. The first bending mode shape (e.g., of the undamaged state) is shown in Fig. 5.

3. DAMAGE DETECTION MODEL

3.1 Theory

For a linear skeletal structure with NE elements and N nodes, damage can be localized using damage indicators which consist of modal parameters derived from experimental measurements and

certain geometric characteristics of the structure[6]. When *nm* vibrational modes are available, a damage localization indicator β_j for the jth member is obtained as follows (See Ref. [6] for details):

$$\beta_j = \sum_i^{nm} f_{ij}^* \Big/ \sum_i^{nm} f_{ij} \; ; \quad \beta_j \geq 0 \tag{1}$$

where f_{ij} and f_{ij}^* represent, respectively, the contribution of the jth location to the ith modal energy for an undamaged state and a sequentially damaged state of the structure.

The predicted location j is classified into one of two groups (i.e., undamaged and damaged locations). First, the values of the indicator β_j (j=1,..., nm) are normalized according to the rule

$$Z_j = \beta_j - \overline{\beta} / \sigma_\beta \tag{2}$$

in which the terms $\overline{\beta}$ and σ_β represent, respectively, the mean and the standard deviation of the collection of β_j values. Next, the damage pattern is classified via a statistical pattern recognition technique using hypothesis testing[7]. The null hypothesis (i.e., H_0) is: the structure is not damaged at the jth location. The alternate hypothesis (i.e., H_1) is: the structure is damaged at the jth location. We select this decision rule as follows:

$$\textbf{Choose } \mathbf{H_1}\textbf{: when } \mathbf{Z_j \geq K}\textbf{; Choose } \mathbf{H_0}\textbf{: when } \mathbf{Z_j < K} \tag{3}$$

in which K is a number that reflects the level of significance of the test (e.g., if K=2, then the probability level of confidence is 0.976).

3.2 Euler-Bernoulli Beam Model

As a damage detection model (i.e., a mathematical representation of a structure with degrees of freedom limited corresponding to a sensor readings) of the test structure, the Euler-Bernoulli beam model was selected on the basis of the following two reasons: first, the girders of the bridge are essentially beams and next, the accelerometers mounted on the girders measure only vertical motion and thus the data collected provide information that could be utilized by a one-dimensional beam.

The fraction of modal energy for the Euler-Bernoulli beam model of the ith mode and the jth location between locations $(x_k,\ x_k + \Delta x_k)$ is computed by

$$f_{ij} = E_j I_j \int_{x_k}^{x_k+\Delta x_k} \{\phi_i''(x)\}^2 dx \Big/ \int_0^L E(x) I(x) \{\phi_i''(x)\}^2 dx \tag{4}$$

and for the damaged structure

$$f_{ij}^* = E_j^* I_j^* \int_{x_k}^{x_k+\Delta x_k} \{\phi_i''^*(x)\}^2 dx \Big/ \int_0^L E(x)^* I(x)^* \{\phi_i''^*(x)\}^2 dx \tag{5}$$

where the quantities E_j and I_j are, respectively, the elastic modulus and the second moment of area of the jth location. Also, ϕ_i and ϕ_i^* are the pre-damage and post-damage ith mode shape vectors, respectively. The asterisks stand for the damaged structure. The equivalent expression for the damage localization indicator is given for each potential damage location j by using post-processed and normalized mode shapes and substituting Eqs. 4 and 5 into Eqs. 1 and 2.

The damage detection model for the test structure is schematized in Fig. 6. The damage detection model includes 846 beam elements of equal size (i.e., the elements NE1-NE423 between the sensors N1 and N13 and the elements SE1-SE423 between the sensors S1 and S13). Note that each element represents a damage detection location and spaces approximately 1 foot (approximately 30 cm) long. In other words the resolution of the damage detection algorithm for this problem is 1 foot or 0.12 percent

(i.e., (1/846) x 100). The use of a 1-foot wide beam element is justified by interpolating pseudo sensor readings at the locations of the 848 nodes (424 nodes each in South and North girders) of the damage detection model obtained via the use of spline functions and the element modal amplitude values.

3.3 Experimental Verification

To check the feasibility of using the damage localization theory to detect and locate damage in structures, a group of verification tests have been performed on numerical examples as well as laboratory-controlled structures. The demonstrations of those tests are fully described in References [6] and [8]. On a limited basis, the practicality of the approach has also been demonstrated by using data from experimental models (See Ref. [6] for details).

4. DAMAGE DETECTION IN TEST STRUCTURE

4.1 Damage Prediction

For each case of the four damage stages, the damage inflicted in the bridge was predicted in four steps. In Step One, we selected modal parameters of the test structure. The modal data (i.e., pre-damage and post-damage modal parameters of the first flexural mode in which each point on the mode shape plot was described by the vertical y displacement) were identified from Table 1 and Fig. 5. In Step Two, we computed the indicator Eq. 1 for damage localization. In Step Three, we established the criterion for Eq. 3 as follows: (1) select H_0 if $Z_i < 3$ (i.e., no damage exists at member i) and (2) select the alternate H_1 if $Z_i \geq 3$. This criterion corresponds to a one-tailed test at a significance level of 0.002 (i.e., 99.8 percent confidence of occurrence). Four, we implemented this criterion to select potential damage locations. The damage localization results for two cases (Case 1 and Case 4) are shown in Figs. 7 and 8 and all results are further listed in Table 2.

Noting that the true damage location in the test structure corresponds to Element NE212 (shown in Fig. 6), we observed that (1) for each of the four damage stages, the resolution of the damage localization ranged from 1.2 to 3.6 percents (i.e., 10-30 feet) and (2) all of the damage cases were correctly predicted. Note that a single mode with 26 actual sensor readings was used to predict potential damage in 846 locations (i.e. 846 elements) via pseudo sensor readings at 848 nodes generated from the use of the cubic spline interpolation. Note also that the resolution of the damage prediction depended upon the use of the pseudo sensor readings.

4.2 Quantification of Damage Prediction Accuracy

The accuracy of the damage prediction results was quantified by measuring both metrical errors and common errors used in tests of hypotheses. We first selected a mean localization error (MLE) defined as

$$MLE(t,f) = \frac{1}{N}\sum_{i=1}^{N} \left| x_i^t - x_i^f \right| / L \quad , \quad 0 \leq MLE(t,f) \leq 1 \tag{13}$$

where N is the number of damage cases, x_i^t is a true location of i^{th} damage case, x_i^f is a false location of i^{th} damage case, and L is a characteristic distance. If MLE=0, then there is no error. If MLE=1, then the damage localization is a maximum.

As the second measure, we selected a detection missing error (DME) defined as

$$DME(t,f) = \frac{1}{NT}\sum_{i=1}^{N} \varepsilon_i^f \,, \quad 0 \leq DME(t,f) \leq 1 \tag{14}$$

in which NT is the number of true damage locations and ε_i^I is a Type I localization error (i.e., ε_i^I=0 if i^{th} damage location is predicted or $\varepsilon_i^I = 1$ if otherwise). If DME=0, then all true damage locations are correctly predicted.

As the last measure, we selected a false alarm error (FAE) defined as

$$FAE(t,f) = \frac{1}{NF}\sum_{i=1}^{N}\varepsilon_i^{II} \ , \quad 0 \le FAE(t,f) < \infty \tag{15}$$

in which NF is the number of predicted locations, ε_i^{II} is a Type II localization error (i.e., $\varepsilon_i^{II} = 0$ if i^{th} predicted location is true or $\varepsilon_i^{II} = 1$ if otherwise). If $FAE(t,f)$=0, then all predicted locations are truly damaged locations.

We implemented the three measures of Eqs. 13-15 to the damage prediction results (e.g., those listed in Table 4) and obtained the accuracy results as follows: MLE=0.0, DME=0.0, FAE=0.43. These results indicate: (1) damage can be predicted without localization (position) error; (2) all of four true damage locations can be predicted (i.e., none of true locations is missed); and (3) three out of seven predicted locations can be false-positive (i.e., no extra locations are alarmed).

5. CONCLUDING REMARKS

From the results of the study, the practicality of the damage detection model has been demonstrated for a real plate-girder bridge. Further research efforts are needed in several directions. Firstly, it is necessary to develop a practical method to estimate the severity of damage in real, full-scale, highway bridges. Secondly, it is necessary to develop a methodology to locate and size damage in real, full-scale, highway bridges for which no as-built modal information are available. Thirdly, it is also necessary to assess the inevitable effect of uncertainty in modeling and modal data on the accuracy of damage prediction results in real structures.

6. REFERENCES

1. Gudmunson, P. (1982). "Eigenfrequency Changes of Structures Due to Cracks, Notches or Other Geometrical Changes", *J. Mech. Phys. Solids*, Vol. 30, No. 5, pp. 339-353.
2. Cawley, P., and Adams, R.D. (1979). "The Location of Defects in Structures from Measurements of Natural Frequencies", *J. Strain Analysis*, Vol. 14, No. 2, pp. 49-57.
3. Kenley, R.M., and Dodds, C.J. (1980). "West Sole WE Platform: Detection of Damage by Structural Response Measurements", *Offshore Tech. Conf.*, Houston, Texas, pp. 111-118.
4. Biswas, M., Pandey, A.K., and Samman, M.M. (1990). "Modal Technology for Damage Detection of Bridges", *NATO Advanced Research Workshop on Bridge Evaluation, Repair and Rehabilitation*, ed. A. Nowak, Kluwer Academic Publishers, Maryland, pp. 161-174.
5. Chen, J., and Garba, J.A. (1988). "On-Orbit Damage Assessment for Large Space Structures", *AIAA Journal*, Vol. 26, No. 9, pp. 1119-1126.
6. Kim, J.T., and Stubbs, N. (1995). "Model Uncertainty and Damage Detection Accuracy in a Plate-Girder Bridge", *Journal of Structural Engineering*, ASCE, Vol. 121. No. 10.
7. Gibson, J.D., and Melsa, J.L. (1975). "Introduction to Nonparametric Detection with Applications", Academic Press, New York.
8. Kim, J.T., and Stubbs, N. (1995). "Damage Detection in Offshore Jacket Structures From Limited Modal Parameters", *Int. J. Offshore and Polar Engineering*, ISOPE, Vol. 5, No. 1, pp. 58-66.

Table 1. First Bending Mode Shape Data for Reference and Four Damaged Cases (natural frequencies Reference (2.48 Hz), Case 1 (2.52 Hz), Case 2 (2.52 Hz), Case 3 (2.46 Hz), and Case 4 (2.30 Hz).

Sensor Number	Case					Sensor Number	Case				
	Ref.	1	2	3	4		Ref.	1	2	3	4
S1	-.006	-.003	-.004	-.004	-.014	N1	-.008	-.007	-.031	-.019	-.028
S2	-.184	-.182	-.198	-.189	-.171	N2	-.212	-.209	-.194	-.197	-.148
S3	-.267	-.268	-.277	-.279	-.243	N3	-.281	-.296	-.289	-.282	-.213
S4	-.214	-.215	-.216	-.218	-.187	N4	-.228	-.222	-.227	-.214	-.169
S5	.000	-.050	-.032	-.020	-.022	N5	-.005	-.103	-.116	-.022	-.010
S6	.375	.380	.373	.368	.346	N6	.394	.393	.385	.384	.364
S7	.616	.613	.600	.602	.625	N7	.591	.589	.594	.593	.703
S8	.401	.411	.417	.404	.426	N8	.394	.196	.306	.107	.390
S9	.012	.012	.104	.101	.012	N9	.110	.115	.112	.112	.116
S10	-.230	-.224	-.223	-.236	-.222	N10	-.211	-.221	-.218	-.214	-.183
S11	-.267	-.263	-.268	-.277	-.301	N11	-.281	-.208	-.287	-.297	-.249
S12	-.201	-.192	-.197	-.206	-.200	N12	-.102	-.169	-.193	-.206	-.164
S13	-.011	-.102	-.008	-.013	-.022	N13	-.012	-.010	-.012	-.010	-.008

Table 2. Comparision of inflicted and predicted location

Damage Case	Inflicted Location	Most Probable Predicted Location(s)	Predicted Range of Damage
1	NE212	NE212, SE212	NE205-NE217, SE204-SE221
2	NE212	NE212, SE212	NE205-NE219, SE220-SE221
3	NE212	NE212, SE212	NE208-NE217, SE204-SE222
4	NE212	NE212	NE201-NE223

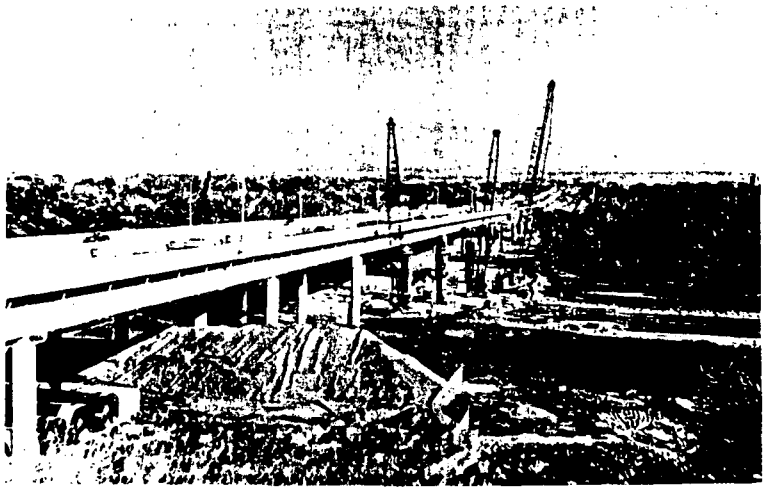

Fig. 1. I-40 Bridge over the Rio Grande in Albuquerque, New Mexico, USA

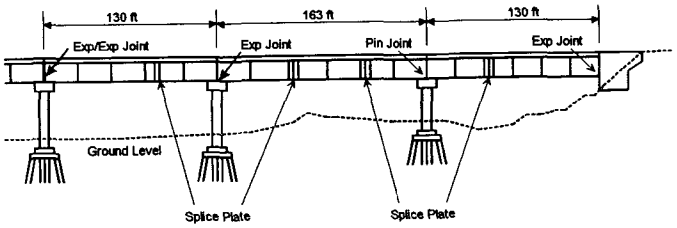

(a) Elevation View

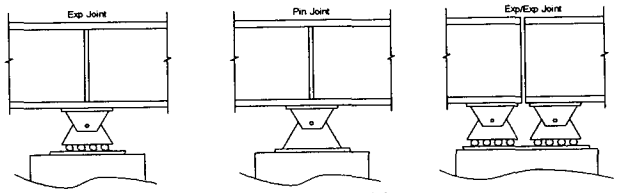

(b) Boundary Conditions

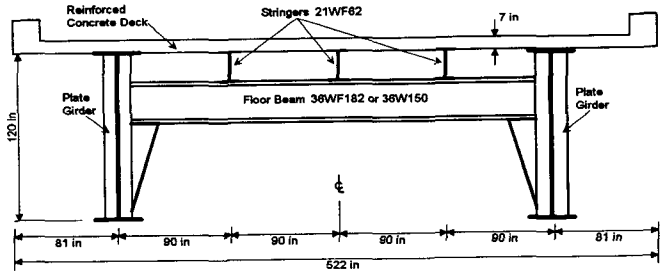

(c) Deck, Floor Beam, and Plate-Girders

Fig. 2. Schematic of the Test Bridge

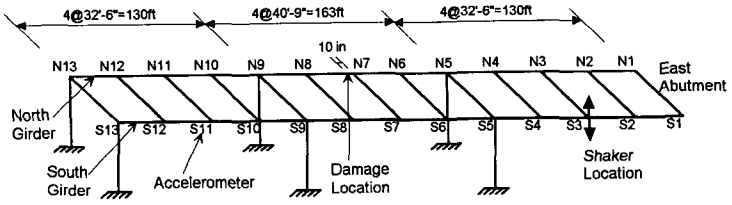

Fig. 3. Accelerometer Locations and Location of Damage

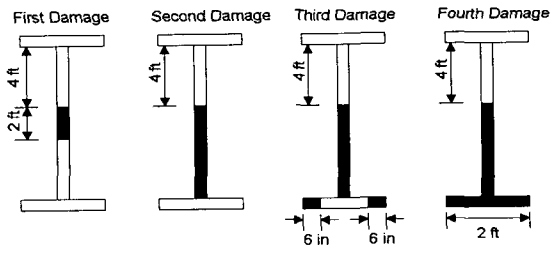

Fig. 4. Schematic of Damage Inflicted in the Test Bridge

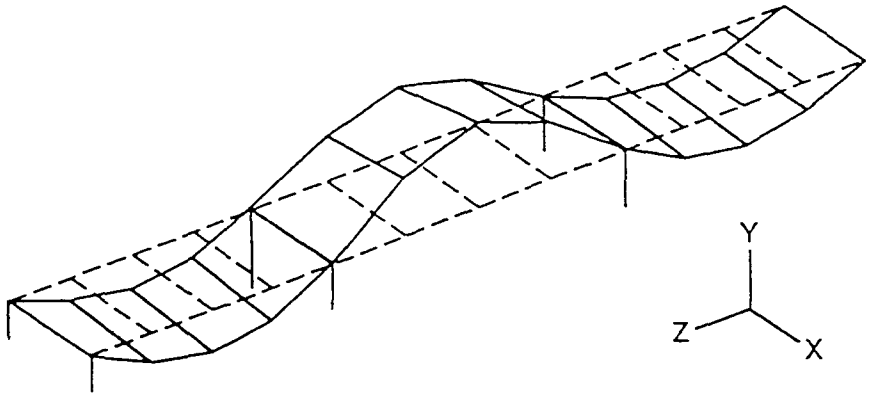

Fig. 5. First Bending Mode of the Undamaged State of the Test Structure

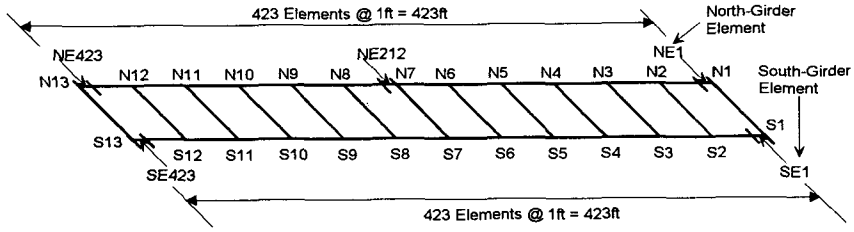

Fig. 6. Schematic of the Damage Detection Model

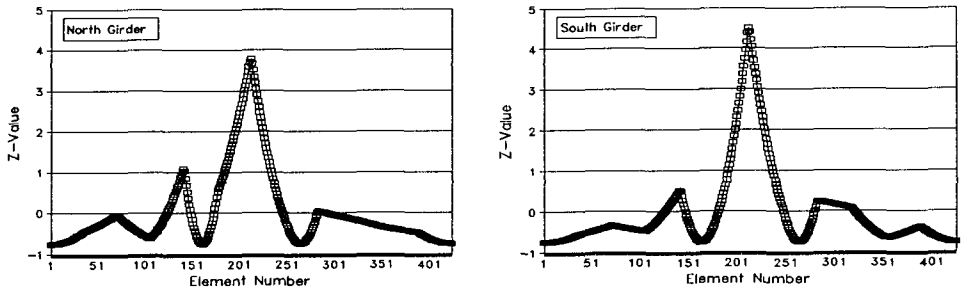

Fig. 7. Damage Localization Results for Damage Case 1

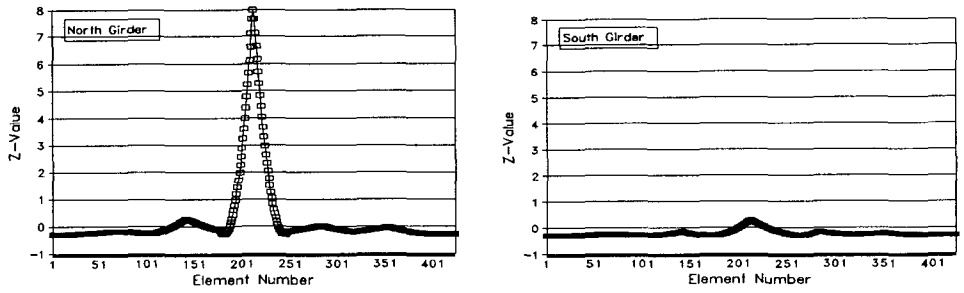

Fig. 8. Damage Localization Results for Damage Case 4